Journal of Nanobiotechnology

RESEARCH

Open Access

Engineering exosomes derived from TNF-α preconditioned IPFP-MSCs enhance both yield and therapeutic efficacy for osteoarthritis

Jiangyi Wu[1†], Jinhui Wu[2†], Wei Xiang[3†], Yunquan Gong[3,4], Daibo Feng[3], Shunzheng Fang[3], Yaran Wu[5], Zheng Liu[2], Yang Li[6], Ran Chen[6], Xiaoqi Zhang[3], Bingfei Li[3], Lifeng Chen[3], Runze Jin[3], Song Li[7], Bin Zhang[7,8], Tongyi Zhang[9], Lin Yin[1], Yizhao Zhou[2], Shu Huang[2], Ningning Liu[10], Hao Xu[11], Jiqin Lian[5], Yongqian Wang[1*], Siru Zhou[6*] and Zhenhong Ni[3*]

Abstract

Background The pathogenesis of osteoarthritis (OA) involves the progressive degradation of articular cartilage. Exosomes derived from mesenchymal stem cells (MSC-EXOs) have been shown to mitigate joint pathological injury by attenuating cartilage destruction. Optimization the yield and therapeutic efficacy of exosomes derived from MSCs is crucial for promoting their clinical translation. The preconditioning of MSCs enhances the therapeutic potential of engineered exosomes, offering promising prospects for application by enabling controlled and quantifiable external stimulation. This study aims to address these issues by employing pro-inflammatory preconditioning of MSCs to enhance exosome production and augment their therapeutic efficacy for OA.

Methods The exosomes were isolated from the supernatant of infrapatellar fat pad (IPFP)-MSCs preconditioned with a pro-inflammatory factor, TNF-α, and their production was subsequently quantified. The exosome secretion-related pathways in IPFP-MSCs were evaluated through high-throughput transcriptome sequencing analysis, q-PCR and western blot analysis before and after TNF-α preconditioning. Furthermore, exosomes derived from TNF-α preconditioned IPFP-MSCs (IPFP-MSC-EXOs$^{TNF-\alpha}$) were administered intra-articularly in an OA mouse model, and subsequent evaluations were conducted to assess joint pathology and gait alterations. The expression of proteins involved in the maintenance of cartilage homeostasis within the exosomes was determined through proteomic analysis.

Results The preconditioning with TNF-α significantly enhanced the exosome secretion of IPFP-MSCs compared to unpreconditioned MSCs. The potential mechanism involved the activation of the PI3K/AKT signaling pathway in IPFP-MSCs by TNF-α precondition, leading to an up-regulation of autophagy-related protein 16 like 1(ATG16L1) levels, which subsequently facilitated exosome secretion. The intra-articular administration of IPFP-MSC-EXOs$^{TNF-\alpha}$ demonstrated superior efficacy in ameliorating pathological changes in the joints of OA mice. The preconditioning

[†]Jiangyi Wu, Jinhui Wu and Wei Xiang have equally contributed to this work.

*Correspondence:
Yongqian Wang
wangyongqian@psh.pumc.edu.cn
Siru Zhou
zhousiru1025@tmmu.edu.cn
Zhenhong Ni
nizhenhong1986@tmmu.edu.cn
Full list of author information is available at the end of the article

of TNF-α enhanced the up-regulation of low-density lipoprotein receptor-related protein 1 (LRP1) levels in IPFP-MSC-EXOs$^{TNF-\alpha}$, thereby exerting chondroprotective effects.

Conclusion TNF-α preconditioning constitutes an effective and promising method for optimizing the therapeutic effects of IPFP-MSCs derived exosomes in the treatment of OA.

Keywords Osteoarthritis, Exosomes, TNF-α precondition, Mesenchymal stem cells, Chondrocytes

Graphical Abstract

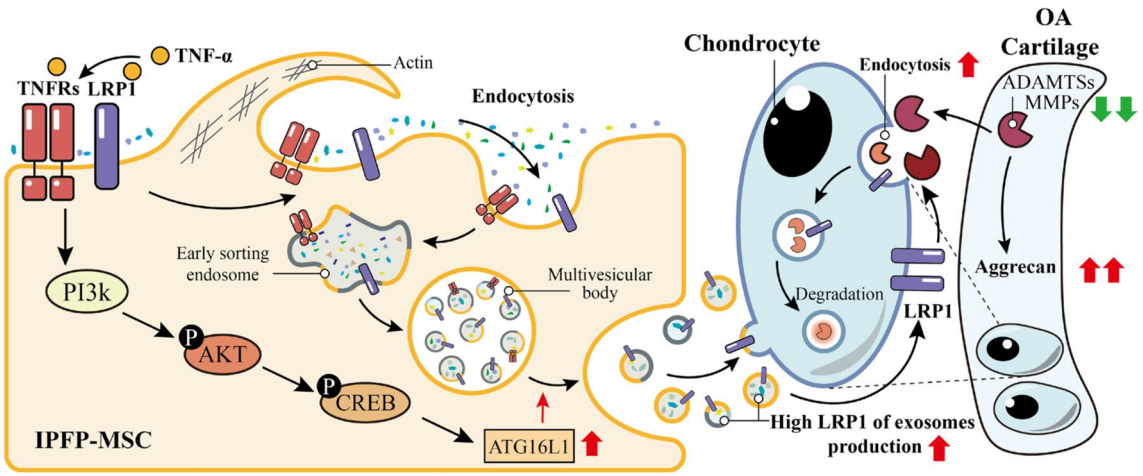

Introduction

The pathogenesis of osteoarthritis (OA) involves the progressive degradation of articular cartilage, accompanied by synovitis, subchondral bone remodeling, and the development of osteophytes [1]. OA encompasses various pathogenic factors, including aging, obesity, gender, occupation, among others. With its global prevalence affecting millions of individuals and being the primary cause of disability worldwide, OA presents a significant challenge to both economic and public health [2]. Currently, pain-relieving medications are commonly administered during the early stages of OA, while joint replacement surgery becomes necessary in advanced cases. Therefore, it is imperative to proactively intervene in or halt the progression of early-stage OA prior to its advancement.

The efficacy of mesenchymal stem cells (MSCs) derived from various sources in mitigating joint pathological injury has been demonstrated in animal models of OA, encompassing the attenuation of cartilage destruction, reduction of synovial inflammation, and mitigation of osteophyte formation [3–5]. However, the direct utilization of MSCs is partially constrained by risk factors such as potential chromosomal variations and immune rejection. Therefore, it is imperative for studies to develop a superior treatment that ensures the effective use of MSCs while mitigating the possible risks associated with their direct application. MSCs-derived exosomes, as an emerging cell-free therapeutic modality, have demonstrated promising therapeutic potential across a range of diseases [6–8]. Our previous study demonstrated that exosomes derived from infrapatellar fat pad (IPFP)-MSCs possess the ability to mitigate cartilage pathological damage by modulating chondrocyte autophagy levels, thereby ameliorating abnormal gait in mice with OA [9]. Enhancing the yield and therapeutic efficacy of exosomes from IPFP-MSCs is a pivotal aspect in facilitating their clinical translation.

The manipulation of MSCs to enhance the therapeutic potential of exosomes presents promising prospects for application, as it allows for controlled and quantifiable external stimulation [10]. Preconditioning MSCs with IL-1β enables the secretion of exosomes containing chondroprotective miRNA cargo and anti-inflammatory factors, facilitating their rapid penetration into collagen-rich regions of cartilage [11, 12]. Additionally, exosomes secreted by lipopolysaccharide (LPS)-preconditioned MSCs significantly enhanced the proliferation and migration of chondrocytes, while inhibiting chondrocyte apoptosis. Moreover, they effectively prevented the

development of the OA mouse model [13]. The results of these experiments demonstrate that the precondition with pro-inflammatory factors can effectively enhance the production of exosomes with chondroprotective properties by MSCs.

The pro-inflammatory cytokine TNF-α plays a pivotal role in orchestrating the inflammatory response in OA [14]. The findings of this study demonstrate that TNF-α preconditioning significantly enhances exosome production in IPFP-MSCs. The activation of the PI3K/AKT signaling pathway leads to the up-regulation of ATG16L1 levels, thereby mediating this effect. Furthermore, proteomic analysis revealed that exosomes from TNF-α preconditioned IPFP-MSCs exhibited elevated levels of low-density lipoprotein receptor related protein 1 (LRP1). LRP1 facilitates the degradation of matrix metalloproteinases (MMPs) and A disintegrin and metalloproteinase with thrombospondin motifs (ADAMTSs) in chondrocytes [15, 16]. The hydrolysis of extracellular matrix (ECM) in articular cartilage is significantly influenced by MMPs and ADAMTSs, thereby effectively protecting ECM from degradation caused by destabilization of the medial meniscus (DMM)-induced OA mouse model in the exosomes from TNF-α preconditioned IPFP-MSCs treatment group.

Methods

Isolation and characterization of IPFP-MSCs

Relevant samples of infrapatellar fat pad and articular cartilage were procured from patients who underwent total knee replacement (TKA) (n = 8). The methodology for sample isolation has been previously documented [9]. Briefly, as for isolation of IPFP-MSCs, the infrapatellar fat pad was harvested and washed in phosphate-buffered saline (PBS, PRC), and then finely diced into small pieces by using a surgical scissor. The diced tissues were digested in 0.2% type I collagenase (Gibco, USA) for 2 h, and the cell suspension was filtered through a 100-μm cell strainer (BD Falcon, USA). The released cells were centrifuged at 400 g for 10 min and resuspended in Red Cell Lysis Buffer (Beyotime, PRC) at room temperature for 10 min. The cells were then centrifuged again, and resuspended in Dulbecco's modified Eagle's medium (DMEM) (Gibco, USA) supplemented with 10% fetal bovine serum (FBS; Gibco, USA) and 1% Penicillin/streptomycin (P/S). The medium was changed every other day. As for isolation of primary articular chondrocytes, cartilage specimens were washed in PBS and then diced. Cartilage tissues were isolated by digesting the matrix overnight in high-glucose DMEM (Gibco, USA) supplemented with 0.2% type II collagenase (Gibco, USA) and 1% P/S. The cell suspension was filtered by a 40-μm cell strainer; and the collected cells were centrifuged at 400 g for 5 min, and then resuspended in high glucose DMEM supplemented with 10% FBS and 1% P/S. The medium was replaced every other day. Cells were used at passage 3. Surface antigens of IPFP-MSCs were characterized by using flow cytometry to detect CD34 (BD Biosciences, RRID: AB_396151, USA), CD45 (BD Biosciences, RRID: AB_10897171, USA), CD73 (BD Biosciences, RRID:AB_393561, USA) and CD105 (BD Biosciences, RRID:AB_2033932, USA).

Flow cytometry analysis

IPFP-MSCs at passage 3 were digested with trypsin and centrifuged. The cells were washed using BD™ Accutase™ Cell Detachment Solution (Cat. No. 561527) and resuspended at a concentration of 5×10^6 cells/ml in BD Pharmingen™ Stain Buffer (Cat. No. 554656). After labeling each tube and adding antibodies according to the instructions, 100 μl of cell suspension was added to the labeled tubes. The tubes were then incubated in the dark at room temperature for 30 min. Following incubation, the cells were washed twice and resuspended in 300 μl BD Pharmingen™ Stain Buffer. Finally, the cells were analyzed using ACEA NovoCyte D2060R flow cytometry analyzer (Agilent USA).

Isolation and identification of exosomes

IPFP-MSCs were washed with PBS twice and cultured in the exosome-free DMEM (Invitrogen, USA). After 48 h, the conditioned medium of IPFP-MSCs was collected for isolation of exosomes. The methods of ultrafiltration were used in this study. Briefly, the conditioned medium of IPFP-MSCs was centrifuged at 300 g for 10 min,1500 g for 10 min and then at 10,000 g for 10 min at 4 °C. After centrifugation, the supernatant was filtered with a 0.22 μm filter (Millipore, USA), which removed the remaining cells and debris effectively. The supernatant was then added to an Ultra-clear tube (Millipore, USA) and centrifuged at 4000 g for 40 min at 4 °C until the volume in the upper compartment was reduced to approximately 200 μl. The ultrafiltration liquid was resuspended in PBS and re-ultrafiltrated at 4000 g to 200 μl. This step was repeated once. Exosomes were stored in aliquots at − 80 °C for further use. For morphology verification of isolated exosomes using Transmission electron microscopy (TEM), the size distribution and concentration of isolated exosomes were determined using a NanoSight LM10 instrument (Malvern, UK).

Transmission electron microscopy (TEM)

The ultrastructure of the MSC-EXOs was identified using TEM (HT-7700, Hitachi, Japan). Briefly, MSC-EXOs samples were diluted with PBS and dropped onto

a copper grid. Filter paper was used to absorb the excess liquid. After staining with uranyl acetate, the grids were air-dried at room temperature and subjected to TEM at 100 kV.

RT-qPCR

Total RNA was extracted from cells using TRIzol Reagent (Invitrogen, USA) and then reverse transcribed into complementary DNA with the PrimeScript™ RT Reagent Kit (Takara, JPN). The samples were then analyzed on the Mx3000P system (Stratagene, USA) by using SYBR Premix Ex Taq™ II Kit (Takara, JPN). GAPDH was used as an internal reference.

Sequences of primers were listed as follows:

	Forward primer	Reverse primer
Rab5	5′- ACTTCTGGGAGAGTC CGCT -3′	5′- TGGGTTAGAAAAGCAGCC CC -3′
Rab7a	5′- CTCTCGGTGTGGCCTTCT AC -3′	5′- GGGTTTTGAATGTGTTGG GGG -3′
Rab27a	5′- AGTTGATGGAGCGAACTG CTT -3′	5′- ACTTCCAATCACATGTCC TCTTCA -3′
ATG5	5′- AGGCACACCACTGAAATG GC -3′	5′- AGATGGACAGTGCAGAAG GTC -3′
SNAP23	5′- CTGCCCATGTAATAGAAC AAAGAAC -3′	5′- TGGTTGCTGAAGCTGACC AT -3′
ATG16L1	5′- CAGAGCAGCTACTAAGCG ACT -3′	5′- AAAAGGGGAGATTCGGAC AGA -3′
GAPDH	5′- CAGGAGGCATTGCTGATG AT -3′	5′- GAAGGCTGGGGCTCA CTT -3′

Western blot

The protein samples were harvested from cell lysates using RIPA (Beyotime, PRC), and the protein concentrations were measured using a BCA protein assay kit (Beyotime, PRC). Western blot analysis was carried out as described previously[9]. The primary antibodies used for Western blotting included anti-ATG16L1 (Proteintech, RRID: AB_2918308, PRC), anti-GAPDH (Proteintech, RRID:AB_2107436, PRC), anti-β-actin (ABclonal, RRID:AB_2768234, PRC) and anti-phospho-AKT (Cell Signaling Technology, RRID:AB_2315049, USA), Densitometry for western blotting was measured using Image J.

RNA-seq analysis

For transcriptome sequencing analysis, IPFP-MSCs were cultured with TNF-α conditioned medium and control medium for 48 h, respectively. Then, the total RNA of IPFP-MSCs was extracted using TRIzol reagent (Invitrogen, USA). The RNA samples were sent for library preparation and the transcriptome sequencing was performed on the NovaSeq X Plus platform by Majorbio company. Briefly, the samples were quantified using Qubit 4.0 and mixed according to the data ratio for sequencing. Bridge PCR amplification was then performed on cBot to generate clusters, and sequencing was finally carried out on the machine. The data were analyzed using the free online Majorbio Cloud Platform, with analyses including GO and KEGG pathway enrichment.

Lentiviral transduction

Human ATG16L1-silencing RNA (ATG16L1-RNAi) was purchased from the Genechem (Shanghai, PRC). ATG16L1-specific siRNA-targeting coding sequences was cloned into GV115 vectors to produce ATG16L1-knockdown vectors. The non-targeting negative control sequence was cloned into the GV115 vectors to construct the ATG16L1-control vectors. Transfection of ATG16L1-RNAi was accomplished according to the manufacturer protocol. The ATG16L1-control vectors transfected IPFP-MSCs were used as controls. Then the transfection efficiency was assessed by immunofluorescence, and the transfected cells were collected to evaluate transfection effectiveness via western blotting.

Quantitative proteomic analysis

To determine the proteomic profiles of exosomes derived from IPFP-MSCs (IPFP-MSC-EXOs), exosomes derived from TNF-α preconditioned IPFP-MSCs (IPFP-MSC-EXOs$^{TNF-\alpha}$) and exosomes derived from naive IPFP-MSCs (IPFP-MSC-EXOs^{naive}) were analyzed using label-free quantification on a liquid chromatography tandem mass spectrometry (LC–MS/MS) system supported by Wayen Biotechnologies following a standard protocol. Firstly, purified exosomes were lysed in protein lysis buffer, and the protein concentration was determined using the BCA method. Secondly, the protein solution samples were digested using the standard filter aided proteome preparation protocol. Thirdly, after centrifugation and drying, the peptides were desalted using a Ziptip C18 column. Once dried, they were used for mass spectrometry analysis. Finally, LC–MS/MS was performed with a QE-HF-X (Thermo Scientific, USA) mass spectrometer. Briefly, after vacuum drying, the samples were reconstituted in 0.1% formic acid (FA), separation was performed at a flow rate of 300 nL/min using an EASY-nLC 1200 system (Thermo Scientific, USA) with a C18 analytical column (2 μm particle size, 100 Å, 50 μm×15 cm, nano Viper). Mass spectrometry analysis was conducted using data-dependent acquisition (DDA) mode. The full scan resolution was set to 60,000 (FWHM) over a mass range of m/z 350–2000. Higher-energy collisional dissociation (HCD) fragmentation was employed with collision energy set to 28%. Raw data were processed by MaxQuant (v 1.5.8.3) with reverse and potential contaminant

proteins removed. Proteins found in exosomes of different groups were compared and then subjected to the differential analysis.

Intra-articular injection of exosomes in an OA mouse model

All animal experiments were conducted in accordance with the regulations of the Animal Research Committee of the Third Military Medical University (Army Medical University). OA was induced in the right knee joints of mice by DMM surgery as described in our previous research [9]. The DMM surgery involved surgically sectioning the medial meniscotibial ligament, while the sham operation only involved incisions in the cutaneous and muscular planes. Four weeks post-surgery, the mice in the DMM + PBS group received intra-articular injections of 10 μl PBS, while those in the DMM + IPFP-MSC-EXOs^{naive} group were administered intra-articular injections of 10 μl IPFP-MSC-EXOs^{naive} (5×10^{10} particles/ml). Additionally, the mice in the DMM + IPFP-MSC-EXOs$^{TNF-\alpha}$ group were subjected to intra-articular injections of 10 μl IPFP-MSC-EXOs$^{TNF-\alpha}$ (5×10^{10} particles/ml). The injections were administered at an interval of every other week until eight weeks post-surgery.

Gait analysis

The gait analysis of freely moving mice was assessed after ten weeks post-surgery using the video-based CatWalk gait analysis system, as previously described [9]. The gait changes of mice were quantified and analyzed using the CatWalk software.

Micro-CT scanning

Ten weeks post-DMM surgery, the right knee joints of mice from different experimental groups were isolated and fixed using 4% paraformaldehyde for a duration of 48 h. The knee joints were imaged using micro-computed tomography (Bruker, Germany). The scanner was configured with a resolution of 15 μm, operating at 70 kV voltage and 200 μA current. Each sample was assessed using consistent thresholds. Three-dimensional structural parameters, including osteophyte morphology and size, were analyzed.

Safranin O/fast green staining

Knee joint sections of mice were stained with the safranin O solid green staining kit (Solarbio, PRC) to observe their cartilage damage [9]. The Osteoarthritis Research Society International (OARSI) scoring system was used to score cartilage damage. According to the OARSI scoring recommendations, the histological changes in the cartilage of the tibiofemoral joint in the medial knee were rated on a scale of 0–6 [9, 17]. In simple terms: 0 = Normal articular cartilage; 0.5 = Loss of articular cartilage matrix; 1 = Small fibrosis of articular cartilage; 2 = Small fissure in the surface layer of articular cartilage; 3 = Articular cartilage fissure or wear range less than 25% of the cartilage surface; 4 = Articular cartilage fissure or wear range affecting 25%-50% of the cartilage surface; 5 = Articular cartilage fissure or wear in the range of 50%-75% of the cartilage surface; 6 = Articular cartilage fissure or wear greater than 75% of the cartilage surface. After scoring 5 slices of each joint, the final statistical metric was the maximum scores and the sum scores of the four highest scores.

H&E staining

Mice knee sections were stained using the H&E staining kit (Solarbio, PRC). The scoring method reported in the literature was used to score the synovitis of mice [17]. In simple terms, it was rated 0–9 based on the histological changes in the synovium of mice. The main evaluation indicators were the number of cell layers in the synovial lining layer (0–3 points), the density of synovium-resident cells (0–3 points), and the infiltration density of inflammatory cells (0–3 points). The sum of these three scores was used for statistical analysis.

Immunohistochemical and immunofluorescence analyses

The knee joint sections of mice were immunostained using commercially available SABC kits (Boster, PRC) following the manufacturer's instructions, as previously described [9]. Briefly, the samples were deparaffinized, followed by quenching with hydrogen peroxide. Subsequently, trypsin treatment was performed and blocked using goat serum. The samples were then incubated with primary antibodies and secondary antibodies. Visualization was achieved using AEC kits (Boster, PRC), followed by counterstaining with hematoxylin. Primary antibodies against the following proteins: LRP-1 (Proteintech, RRID: AB_3085841, PRC) and Aggrecan (Proteintech, RRID: AB_2722780, PRC). A semi-quantitative cellular scoring was performed utilizing a four-point scale based on immunohistochemical intensity: negative (0), mild positivity (1 +), moderate positivity (2 +), and strong positivity (3 +) [18]. As for the immunofluorescence assay, LRP-1 (Proteintech, RRID:AB_3085841, PRC) was used as primary antibody. After dark-incubating with a fluorescein secondary antibody, chondrocytes were observed using the fluorescent microscope and each collected image was evaluated for fluorescence intensity using ImageJ [9].

Statistical analysis

The experimental data were analyzed using Prism 10.0 software (GraphPad Prism) and presented as mean ± SD.

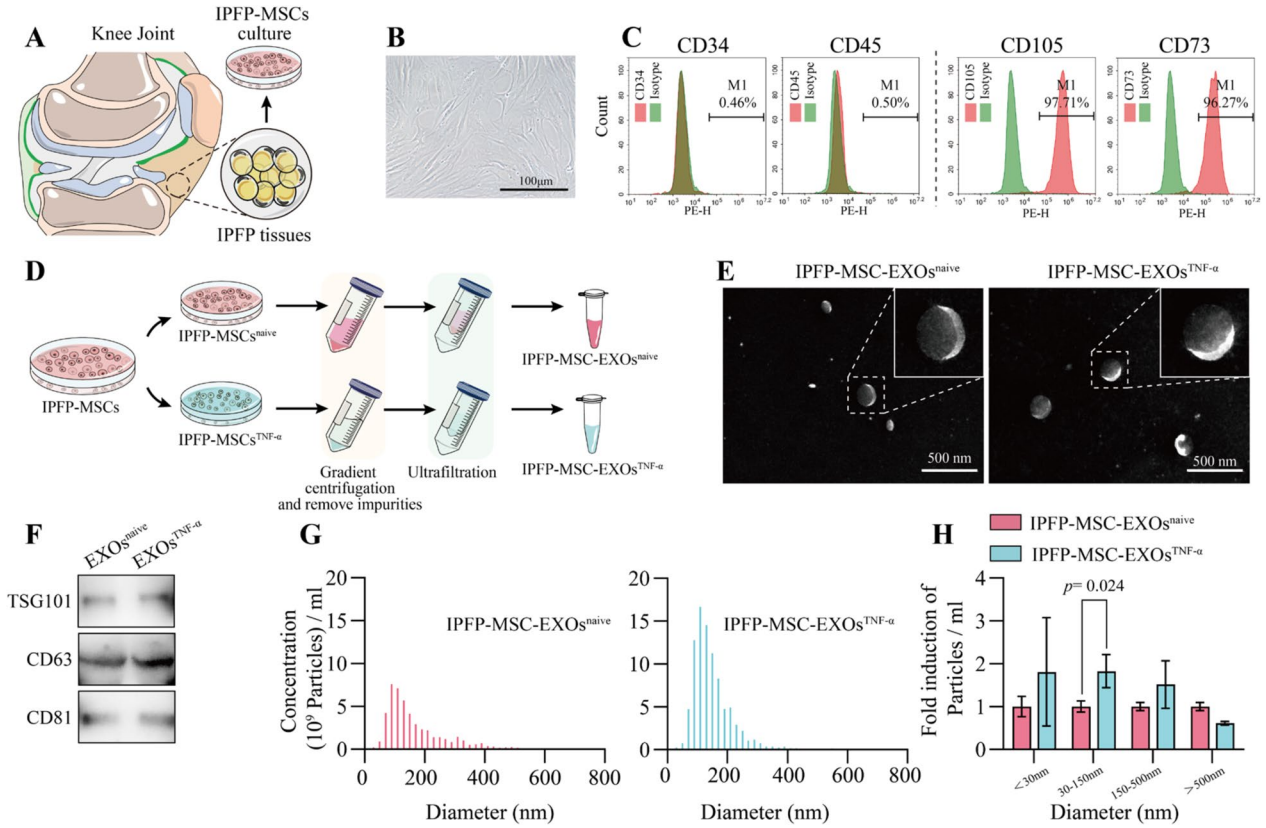

Fig. 1 Characterization of IPFP-MSCs and IPFP-MSC-EXOs. **A** Flowchart of isolation and culture of IPFP-MSCs from OA patients. **B** IPFP-MSCs at passage 3 showed a representative spindle-like morphology under light microscopy. Scale bar: 100 μm. **C** The flow cytometry analysis showed that IFPF-MSCs exhibited low expression of CD34 and CD45, high expression of CD105 and CD73 on their surface. **D** Schematic illustration of IFPP-MSC-EXOs isolation process. **E** The morphology of IFPP-MSC-EXOs^{naive} and IFPP-MSC-EXOs$^{TNF-\alpha}$ exhibited a typical sphere-shaped bilayer membrane structure under transmission electron microscopy (TEM), and the representative image was shown. **F** The western blotting of IFPP-MSC-EXOs^{naive} and IFPP-MSC-EXOs$^{TNF-\alpha}$ exhibited positive expression of TSG101, CD63 and CD81. **G** The size distribution and concentration of IFPP-MSC-EXOs^{naive} and IFPP-MSC-EXOs$^{TNF-\alpha}$ measured by nanoparticle tracking analysis (NTA). **H** The statistical analysis for the size distribution of extracellular vesicles from different samples

The independent-sample t-test was employed to compare two distinct groups, while multiple group comparisons were conducted using ANOVA. Statistical significance was determined at a threshold of $p < 0.05$.

Results

Characterization of IPFP-MSCs and IPFP-MSC-EXOs

The primary IPFP-derived MSCs were isolated from TKA patients and subsequently cultured in cell culture dishes (Fig. 1A). At passage 3 of culture, the representative cells were examined using a light microscope and displayed characteristic spindle-shaped morphology (Fig. 1B). The immunophenotype of IPFP-MSCs was characterized by flow cytometry, demonstrating high expression of stem cell markers, including CD105 and CD73, and absence of hematopoietic lineage markers, such as CD34 and CD45 (Fig. 1C). The IPFP-MSCs were divided into two groups: the control group and the TNF-α preconditioned group. In the TNF-α preconditioned group, IPFP-MSCs were treated with 75 ng/ml TNF-α for 48 h prior to further processing. Subsequently, exosomes were isolated from the supernatant of both TNF-α preconditioned and untreated IPFP-MSCs using an ultrafiltration method employing a commercially available nanomembrane concentrator (Fig. 1D). The exosomes were characterized using TEM and nanoparticle tracking analysis (NTA). Both IPFP-MSC-EXOs^{naive} and IPFP-MSC-EXOs$^{TNF-\alpha}$ showed a morphology characterized by sphere-shaped bilayer membrane structures (Fig. 1E). The NTA analysis revealed that both IPFP-MSC-EXOs^{naive} and IPFP-MSC-EXOs$^{TNF-\alpha}$ exhibited comparable peaks at approximately 150 nm in size (Fig. 1G). The western blotting revealed that both IPFP-MSC-EXOs^{naive} and IPFP-MSC-EXOs$^{TNF-\alpha}$ exhibited positive expression of TSG101, CD63 and CD81 (Fig. 1F). The number of extracellular vehicles (EVs) with diameters ranging from 30 to

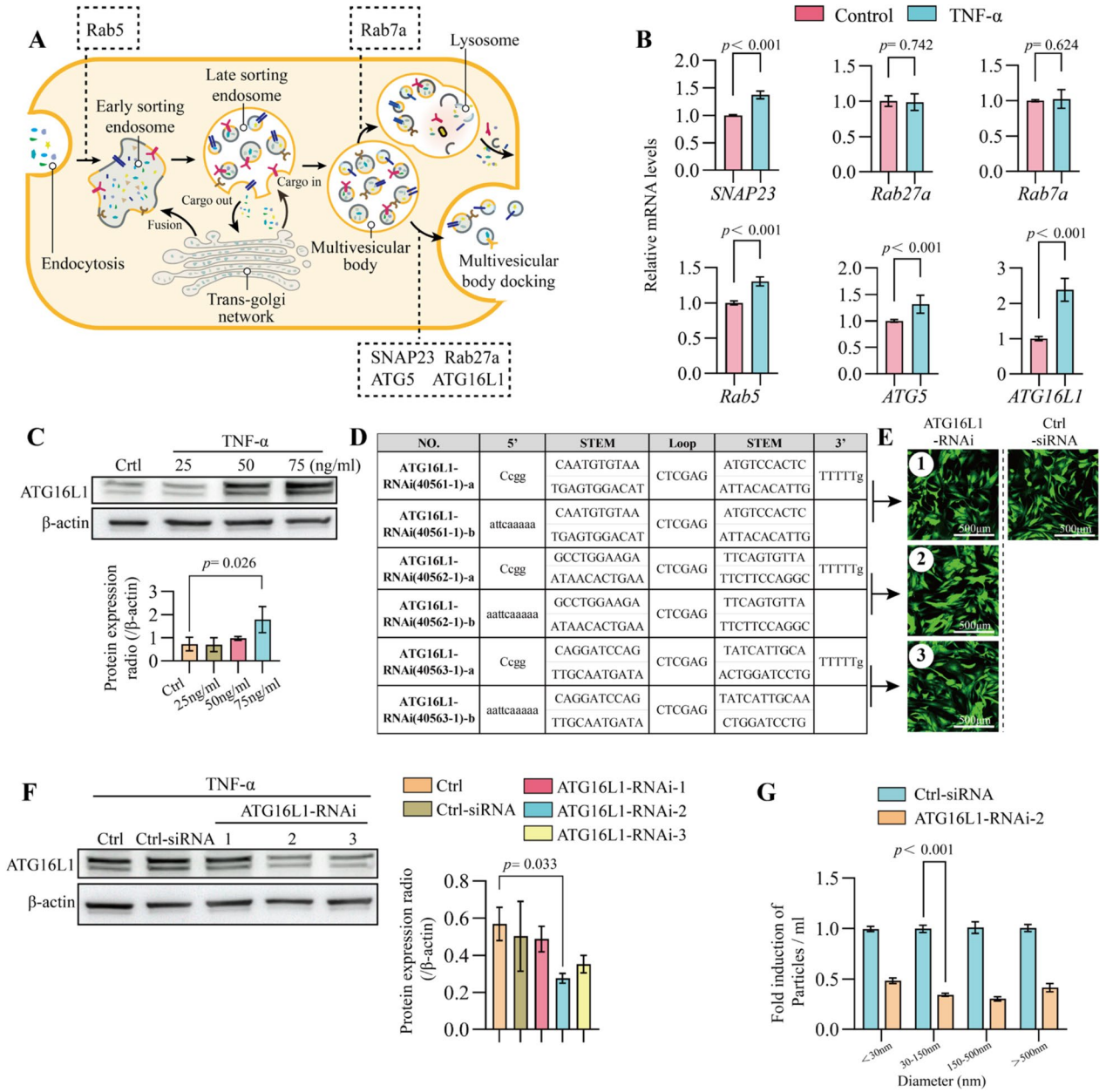

Fig. 2 TNF-α pretreatment enhances the EVs secretion of IPFP-MSC by upregulating ATG16L1. **A** Schematic diagram of exosomes synthesis and release processes. **B** IPFP-MSCs were pretreated with or without 75 ng/ml TNF-α for 24 h, and then the mRNA expression of genes related to exosome synthesis and secretion were detected by RT-qPCR, with ATG16L1 showing the most pronounced changes. **C** The protein levels of ATG16L1 in IPFP-MSCs cultured with TNF-α at indicated concentrations for 48 h were analyzed by western blot assay, and the statistical graph of ATG16L1 protein expression after gradient TNF-α treatment. **D** ATG16L1-RNAi lentiviruses were constructed according to different target sequences. **E** Monitoring of the transfection efficiency of the lentiviruses into IPFP-MSCs using a fluorescence microscope that measured GFP expression. **F** The transfection efficiency of the lentiviruses was detected by western blot assay, and the statistical analysis of ATG16L1 protein expression following lentiviral transfection indicated that ATG16L1-RNAi-2 demonstrated the most effective knockdown efficiency of ATG16L1. **G** Exosomes yield of different groups determined by the NTA

150 nm exhibited a significant increase (approximately 1.8-fold on average) in the control group compared to the TNF-α preconditioned group (Fig. 1H). Moreover, notable alterations were observed in the abundance of EVs within other diameter ranges between these two groups (Fig. 1H). These findings suggest that TNF-α preconditioning enhances the release of EVs by IPFP-MSCs when compared to untreated IPFP-MSCs.

TNF-α precondition enhances the EVs secretion of IPFP-MSCs by upregulating ATG16L1 levels.

To clarify the mechanism that TNF-α induced the promotion of EVs in IPFP-MSCs, a series of molecules including SNAP23, Rab27a, Rab7a, Rab5, ATG5 and ATG16L1, associated with EVs synthesis and secretion, were detected in IPFP-MSCs (Fig. 2A). Firstly, IPFP-MSCs were preconditioned with or without TNF-α (75 ng/ml) for 24 h, the mRNA expression was detected using RT-qPCR assay. The mRNA expression levels of ATG16L1 in IPFP-MSCs were significantly upregulated following TNF-α preconditioning (Fig. 2B). Subsequently, IPFP-MSCs were subjected to preconditioning with various concentrations (25 ng/ml, 50 ng/ml and 75 ng/ml) of TNF-α for 48 h. The subsequent detection of ATG16L1 protein expression was performed using a western blot assay. After treatment with 75 ng/ml TNF-α, the protein levels of ATG16L1 in IPFP-MSCs showed the most significant upregulation (Fig. 2C). To further investigate the potential of TNF-α in enhancing the release of EVs from IPFP-MSCs, we constructed three types of ATG16L1-RNAi lentiviruses to knock down the expression of ATG16L1 (Fig. 2D). IPFP-MSCs were transiently transfected with negative controls or different ATG16L1-RNAi lentiviruses for 3 days, and then preconditioned with 75 ng/ml TNF-α for 48 h. The transfection efficiency in IPFP-MSCs was evaluated using fluorescence microscopy and western blot analysis. The findings revealed that lentiviruses efficiently transfected IPFP-MSCs (Fig. 2E), with the target sequence of ATG16L1-RNAi-2 demonstrating the most significant inhibitory effect on ATG16L1 expression in these cells (Fig. 2F). Furthermore, IPFP-MSCs were transfected with negative controls or ATG16L1-RNAi-2, and then preconditioned with 75 ng/ml TNF-α for 48 h. The exosomes derived from IPFP-MSCs were collected separately and subjected to Nanosight analysis. The data revealed that the ATG16L1-RNAi-2 group exhibited a significantly reduced concentration of EVs compared to the control group (Fig. 2G). Based on these findings, it is plausible that TNF-α preconditioning may enhance the production of EVs in IPFP-MSCs, at least in part, through the up-regulation of ATG16L1 levels.

ATG16L1 expression in IPFP-MSCs is upregulated by TNF-α through the PI3K/AKT signaling pathway

To investigate the molecular pathways underlying the TNF-α-induced up-regulation of ATG16L1 expression, IPFP-MSCs were preconditioned with or without TNF-α for 48 h, followed by collection of cell lysates for high-throughput transcriptome sequencing analysis (Fig. 3A). The transcriptome sequencing data exhibited high quality, demonstrating homogeneity in the results (Fig. 3B). The volcano plot revealed that in the TNF-α preconditioned group, a total of 2752 genes were found to be up-regulated, while 6004 genes exhibited down-regulation (Fig. 3C). The enriched Gene Ontology (GO) analysis revealed that the most significant terms are associated with embryonic skeletal joint morphogenesis (Fig. 3D). The Kyoto Encyclopedia of Genes and Genomes (KEGG) analysis revealed the enrichment of multiple signaling pathways, including the PI3K-AKT pathway, in the TNF-α preconditioned group (Fig. 3E). To further validate the results, IPFP-MSCs were preconditioned with 75 ng/ml TNF-α and the resulting cell lysates were subjected to Western blot analysis (Fig. 3F–G). Previous studies have demonstrated that activation of the PI3K-AKT pathway leads to phosphorylation of various downstream molecules, including cyclic AMP-responsive element binding protein (CREB) [19–21]. According to the database of transcription factor binding site prediction (https://jaspar.genereg.net), it has been identified that the transcription factor CREB exhibits potential binding affinity towards the promoter region of ATG16L1 (Fig. 3H). LY294002, an effective inhibitor of PI3K, has been widely employed as a drug of choice in studies investigating the PI3K/AKT pathway by our group and others [22, 23]. The TNF-α preconditioned IPFP-MSCs were subsequently treated with 40 μM LY294002. Remarkably, the administration of LY294002 resulted in a significant reduction in ATG16L1 mRNA levels within the TNF-α preconditioned IPFP-MSCs (Fig. 3I). The Western blot assay confirmed these observations, showing that AKT pathway inhibitors effectively downregulated the protein levels of ATG16L1 induced by TNF-α in IPFP-MSCs (Fig. 3J).

(See figure on next page.)

Fig. 3 TNF-α upregulates the expression of ATG16L1 in IPFP-MSCs via PI3K/AKT signaling pathway. **A** Flowchart for the transcriptome sequencing analysis. **B** Quality analysis of transcriptome sequencing. **C** A volcano plot of RNA-seq results. **D** and **E** KEGG pathway enrichment analysis and GO enrichment analysis of differentially expressed genes. **F** The protein levels of p-AKT in IPFP-MSCs cultured with 75 ng/ml TNF-α for 48 h were analyzed by western blot assay. **G** Statistical map of p-AKT protein expression after TNF-α. **H** Prediction of CREB binding sites in ATG16L1 promoter region. **I** After treating with 40 μM AKT pathway inhibitor LY294002, the ATG16L1 mRNA levels of TNF-α primed IPFP-MSCs were analyzed by RT-qPCR. **J** TNF-α primed IPFP-MSCs were treated with 20 μM or 40 μM LY294002, and the protein expression of ATG16L1 was determined using western blot analysis

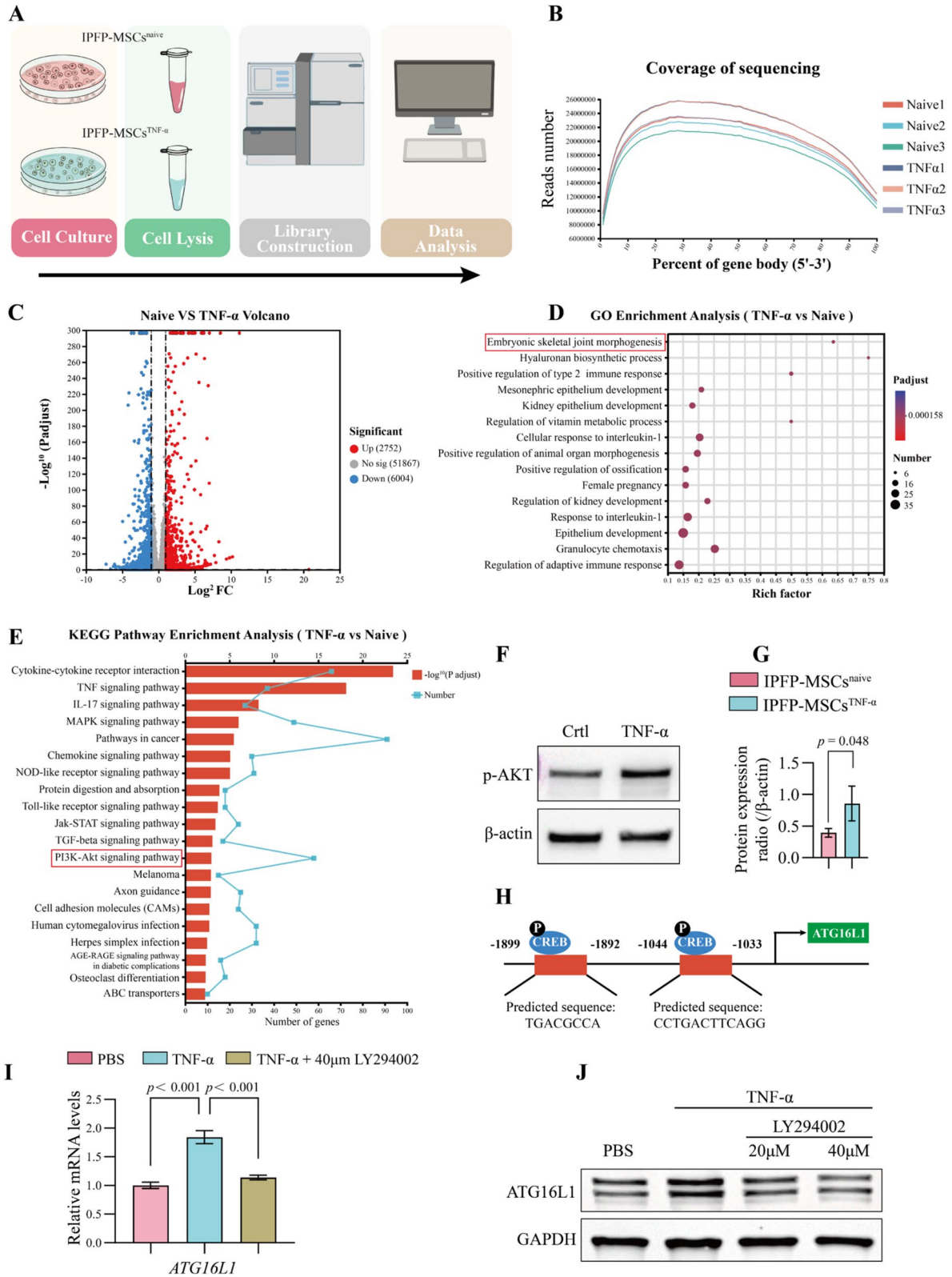

Fig. 3 (See legend on previous page.)

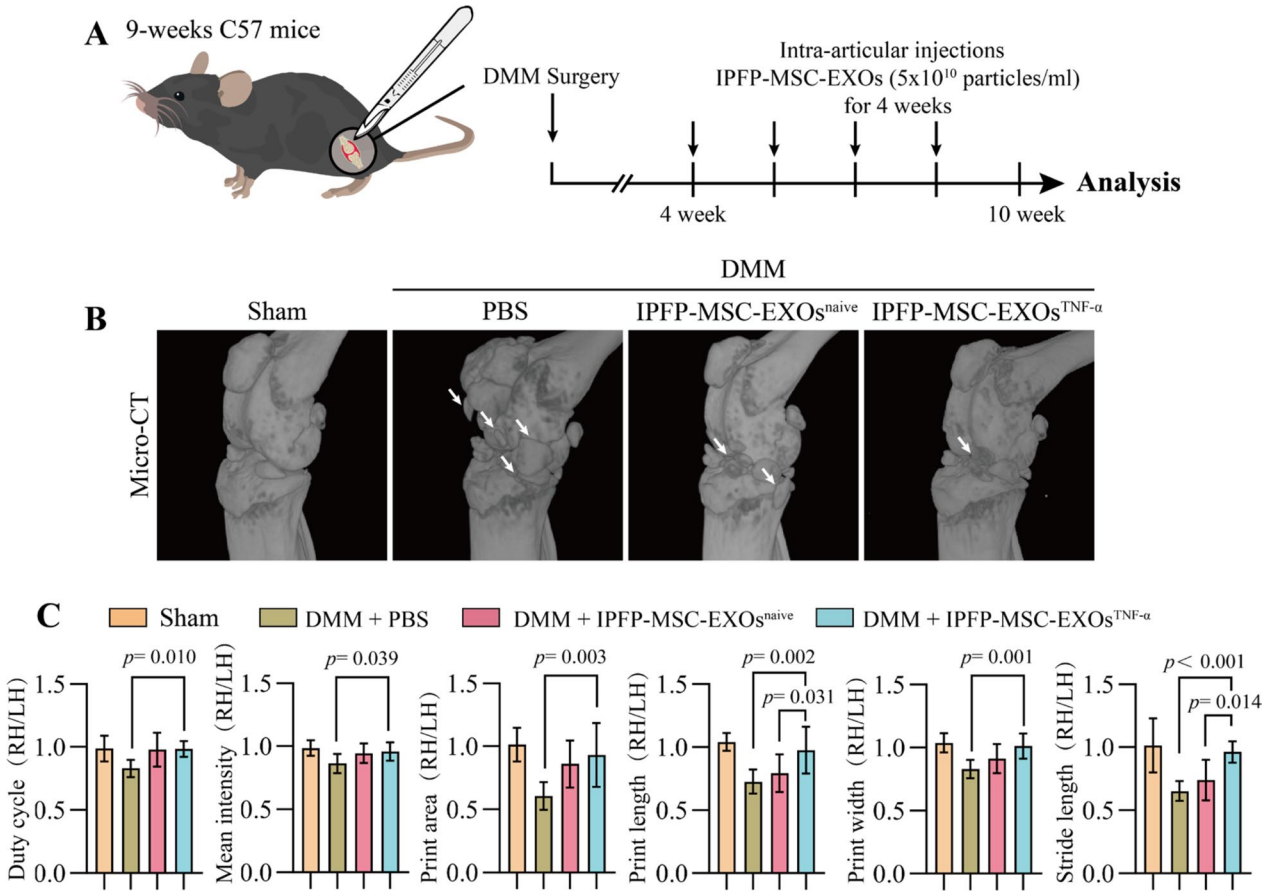

Fig. 4 Therapeutic effects of IPFP-MSC-EXOs$^{TNF-\alpha}$ on OA mice model. **A** Schematic diagram of IPFP-MSC-EXOs$^{TNF-\alpha}$ treatment strategy in OA mice. **B** Representative images of three-dimensional reconstruction of the knees in the different groups by micro-CT. shown in the oblique coronal plane. White arrows: osteophytes. **C** Gait parameters including duty cycle, mean intensity, print area, print length, print width and stride length were compared in different mice groups by Catwalk system. Values are presented as the ratio of the right hind (RH, DMM applied knee)/the left hind (LH, contralateral knee)

The intra-articular administration of IPFP-MSC-EXOs$^{TNF-\alpha}$ demonstrated superior efficacy in ameliorating gait abnormalities and pathological changes compared to that of IPFP-MSC-EXOs^{naive} in the joint of DMM mice

To assess the comparative efficacy of IPFP-MSC-EXOs$^{TNF-\alpha}$ versus IPFP-MSC-EXOs^{naive} in protecting OA joints in vivo, we evaluated the clinical and pathological status in an OA mouse model. Initially, we successfully established an experimental model of OA by inducing it through DMM surgery in 9-week-old male C57 mice. After a 4-week period following the DMM surgery, either PBS or IPFP-MSC-EXOs (at a concentration of 5×10^{10} particles/ml) were administered into the articular cavity of the OA mice once per week for consecutive 4 weeks. Subsequently, the mice were sacrificed after 2 weeks for further analysis (Fig. 4A). The total joints of OA mice were evaluated using micro-computed tomography (Micro-CT). The joints in the Sham group remained intact without the presence of osteophytes, whereas numerous osteophytes were observed within the joint cavity of mice in the PBS injection group. Intra-articular administration of IPFP-MSC-EXOs^{naive} attenuated osteophyte formation in DMM mice, with IPFP-MSC-EXOs$^{TNF-\alpha}$ injection demonstrating superior efficacy in reducing osteophytes (Fig. 4B). Considering the ability of IPFP-MSC-EXOs^{naive} and IPFP-MSC-EXOs$^{TNF-\alpha}$ to mitigate OA pathology in the knee joint, we hypothesized their potential to ameliorate gait pattern abnormalities in mice undergoing DMM surgery. In our previous study, we observed a partial improvement in gait abnormality in the DMM mice model following treatment with IPFP-MSC-EXOs^{naive} [9]. To further investigate the potential effects of IPFP-MSC-EXOs$^{TNF-\alpha}$, we assessed gait parameters, including print length, duty cycle, mean intensity, print area, print width and stride length, using a Catwalk system in different groups of mice. The IPFP-MSC-EXOs$^{TNF-\alpha}$ group exhibited significant improvements in all gait parameters compared to the PBS group.

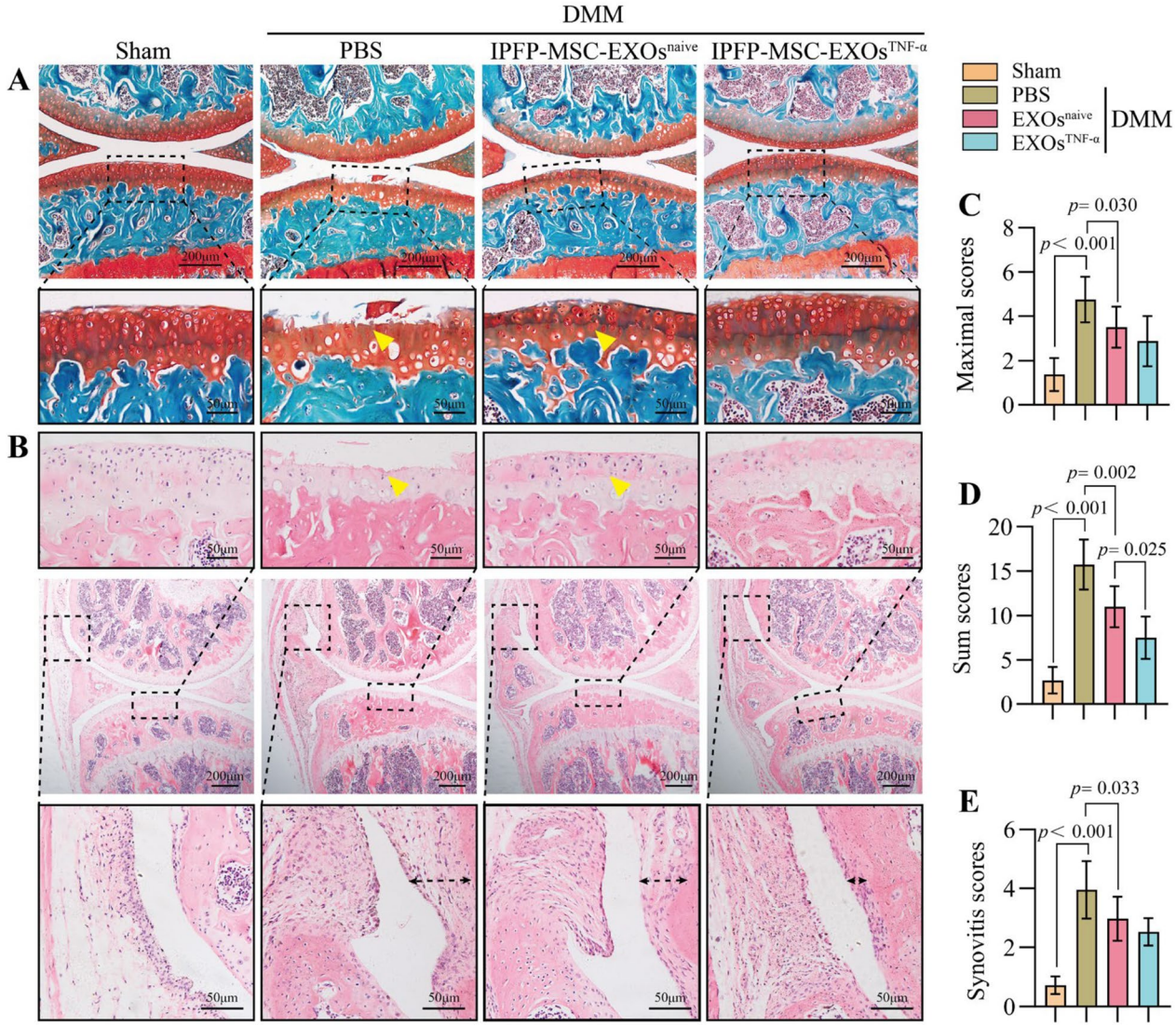

Fig. 5 IPFP-MSC-EXOs$^{TNF-\alpha}$ local injection improves cartilage degradation and synovial inflammation in vivo. **A** Safranin O/fast green staining of cartilage morphology in different OA mice group, dashed boxes were amplified showing articular cartilage destruction (yellow arrowheads). Scale bar: 50 μm. **B** Representative images of H&E staining of the OA mice knee, higher magnification was depicted by dashed boxes (the dashed double-headed arrows represents synovial inflammation). Scale bar: 50 μm. **C** and **D** The OARSI scoring system quantify the severity of cartilage destruction in knee joints of OA mice. n = 8 for each group. **E** Synovial inflammation was evaluated with the synovitis scores. n = 8 for each group

And the IPFP-MSC-EXOs$^{TNF-\alpha}$ group exhibited significant improvements in print length and stride length compared to the IPFP-MSC-EXOs^{naive} group (Fig. 4C). These findings suggest that intra-articular administration of IPFP-MSC-EXOs$^{TNF-\alpha}$ exhibited superior efficacy in alleviating gait abnormalities compared to the administration of IPFP-MSC-EXOs^{naive}.

The degradation of articular cartilage and loss of ECM were investigated using Safranin O-fast green staining. Specifically, basophilic cartilage exhibits a preference for the basic dye Safranin O, which yields a distinct red hue, whereas acidophilic bone readily binds to the acidic dye Fast Green, resulting in a vibrant green coloration. (Fig. 5A). Remarkable destruction of the articular cartilage was observed in the PBS group. Both the IPFP-MSC-EXOs^{naive} group and IPFP-MSC-EXOs$^{TNF-\alpha}$ group exhibited improvements in cartilage repair, with the IPFP-MSC-EXOs$^{TNF-\alpha}$ group showing a more complete cartilage surface. The cartilage degeneration in the medial tibial plateau and medial femoral condyle of mice knee joints was assessed using a scoring system ranging from 0 to 6, following the guidelines recommended by the

Osteoarthritis Research Society International (OARSI) [24]. The scoring system comprises the Summed Score (the sum of the four highest scores from each section within the same joint) and the Maximal Score (the highest score from each section within the same joint). Histological analysis revealed that the IPFP-MSC-EXOs$^{TNF-\alpha}$ group exhibited the lowest OARSI score (Fig. 5C–D), indicating a remarkable therapeutic effect of IPFP-MSC-EXOs$^{TNF-\alpha}$ in mitigating cartilage destruction in mice with OA. The synovial inflammation of mice knee joints was assessed by performing H&E staining (Fig. 5B). The degree of synovial inflammation was assessed by evaluating synovitis scores, which were based on the thickness of cells in the synovial lining layer and the density of cells in the synovial stroma [25]. The PBS group exhibited more severe synovitis, including an enlarged synovial lining cell layer, an increased number of synovial stroma cells, and heightened inflammatory infiltration in the knee joint. Notably, the IPFP-MSC-EXOs$^{TNF-\alpha}$ group displayed a lower synovitis score comparable to that of the IPFP-MSC-EXOs^{naive} group (Fig. 5E).

The proteomic analysis reveals a significant enrichment of exosomal LRP1 in IPFP-MSC-EXOs$^{TNF-\alpha}$

To investigate the underlying mechanism by which TNF-α precondition enhances the therapeutic efficacy of exosomes derived from IPFP-MSCs, we employed high-throughput label-free quantitative proteomic analysis to identify differentially expressed proteins in exosomes isolated from the culture supernatants of IPFP-MSC-EXOs^{naive} and IPFP-MSC-EXOs$^{TNF-\alpha}$ (Fig. 6A). A total of 241 proteins were identified in the two sample groups, with 139 and 227 proteins identified in IPFP-MSC-EXOs^{naive} (Ctrl group) and IPFP-MSC-EXOs$^{TNF-\alpha}$ (TNF-α group), respectively. Notably, we observed an overlap of 125 proteins expressed in both groups, among which 55 proteins were up-regulated and 12 proteins were down-regulated specifically in IPFP-MSC-EXOs$^{TNF-\alpha}$ compared to IPFP-MSC-EXOs^{naive} (Fig. 6B). The mass spectra revealed the predominant proteins in IPFP-MSC-EXOs$^{TNF-\alpha}$, with particular attention drawn to LRP1 (Fig. 6D). The GO terms and KEGG pathways were identified for the differentially upregulated proteins. The results indicated that the most significantly enriched GO terms were primarily associated with ECM-receptor interaction, while the up-regulated proteins exhibited enrichment in KEGG pathways specifically related to ECM organization (Fig. 6C and E). It has been previously reported that LRP1, a transmembrane protein of type I, serves as the primary endocytic receptor for extracellular matrix-degrading MMPs and ADAMTSs in chondrocytes [15, 16] (Fig. 6F).

Exosomal LRP1 protein derived from IPFP-MSC-EXOs$^{TNF-\alpha}$ exerts a chondroprotective effect

In order to investigate the potential association between exosomal LRP1 protein and the therapeutic efficacy of IPFP-MSC-EXOs$^{TNF-\alpha}$, a series of in vivo and in vitro experiments were conducted to validate our hypothesis. The human primary chondrocytes were subjected to a 48 h treatment with both H_2O_2 (200 μM, 48 h) and IPFP-MSC-EXOs$^{TNF-\alpha}$ (1×10^8 particles/ml). Subsequently, the protein levels of LRP1 in chondrocytes were assessed using an Immunofluorescence assay. The results demonstrated a significant upregulation of LRP1 expression in chondrocytes upon treatment with IPFP-MSC-EXOs$^{TNF-\alpha}$ (Fig. 7A, B). The up-regulation of LRP1 in chondrocytes may potentially be attributed to the internalization of IPFP-MSC-EXOs$^{TNF-\alpha}$, indicating a plausible mechanism. In subsequent animal experiments, we evaluated the immunohistochemical expression of LRP1 in the articular cartilage of mice with OA. The expression of LRP1 was found to be up-regulated in the articular cartilage of mice treated with IPFP-MSC-EXOs$^{TNF-\alpha}$, concomitant with increased levels of aggrecan expression (Fig. 7C, D). This suggests that OA chondrocytes may internalize IPFP-MSC-EXOs$^{TNF-\alpha}$, which are rich in LRP1 protein. Furthermore, the exosomal LRP1 protein might play a role in promoting the catabolism of ECM-degrading MMPs and ADAMTSs, indirectly leading to an upregulation of aggrecan expression. This upregulation is associated with maintaining the homeostasis of ECM in cartilage.

(See figure on next page.)

Fig. 6 Effect of TNF-α treatment on IPFP-MSC-EXOs composition. **A** Workflow of the high throughput label-free quantitative proteomic analysis. **B** Venn diagram showing overlap of protein groups identified by label-free quantitative proteomics in the indicated exosomes. **C** KEGG pathway analysis of proteomic data in IPFP-MSC-EXOs. The vertical axis represents the pathway category and the horizontal axis represents pathway's enrichment score [− log10(adjusted P value)]. **D** Heatmap analysis of differentially expressed proteins in IPFP-MSC-EXOs, dashed boxes were enlarged to show the top 13 proteins that up-regulated in IPFP-MSC-EXOs$^{TNF-\alpha}$. **E** Pie diagram of Gene ontology of the differentially expressed proteins was performed to study the specific biological processes (GO-BP). **F** LRP1-mediated endocytic pathway of ECM-degrading metalloproteinases in chondrocyte

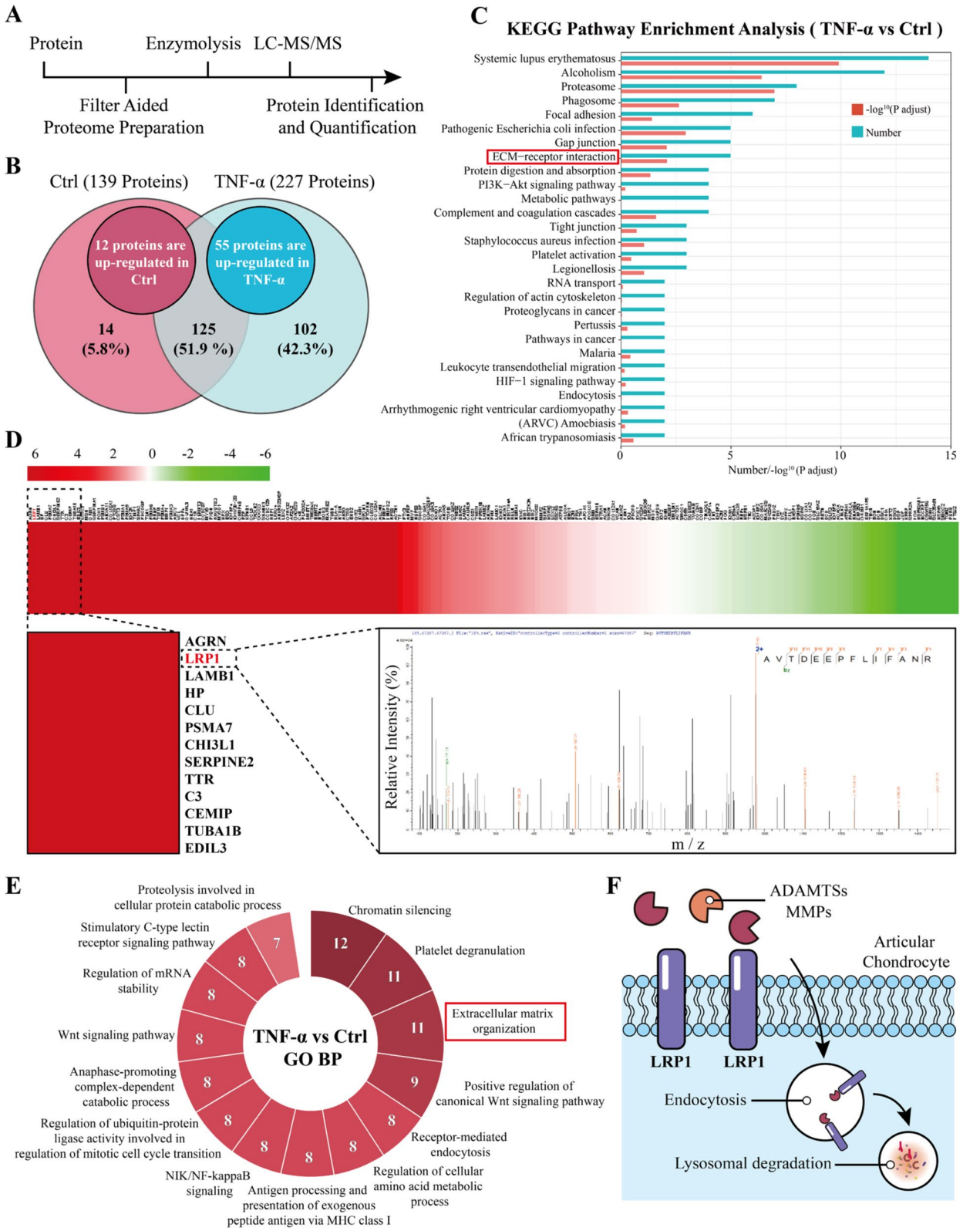

Fig. 6 (See legend on previous page.)

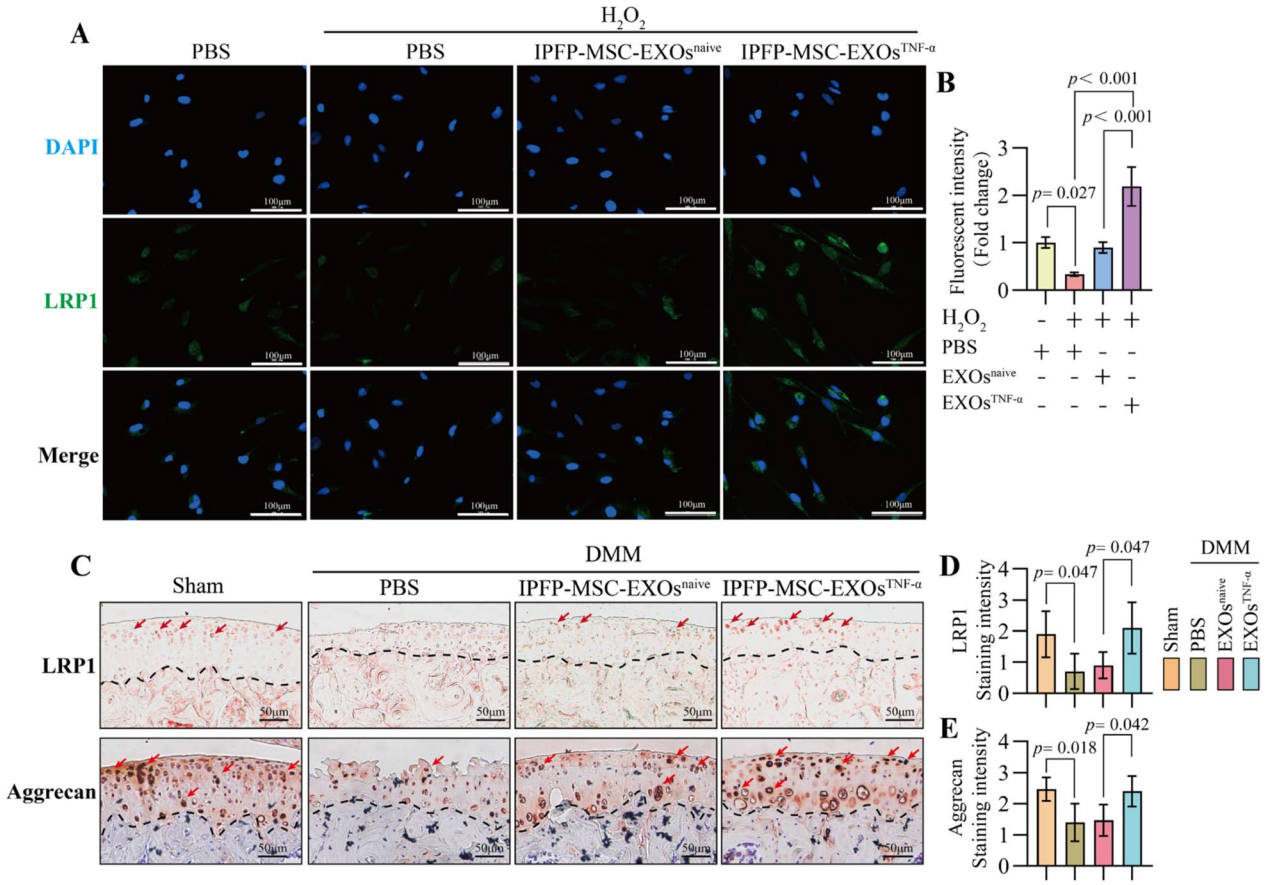

Fig. 7 IPFP-MSC-EXOs$^{TNF-\alpha}$ exert chondroprotective effect through exosomal LRP1 protein. **A** Chondrocytes were induced with H_2O_2 to establish OA model and then treated with IPFP-MSC-EXOs$^{TNF-\alpha}$, the LRP1 protein levels in chondrocytes were analyzed using Immunofluorescence assay. Scale bar:100 μm **B** Statistical evaluation of fluorescence intensity (fold change). n = 3 for each group. **C** Representative images of immunohistochemical staining of aggrecan and LRP1 of cartilage in various groups. The dashed line is used to distinguish between cartilage and subchondral bone and the red arrows indicate the positive chondrocytes. Scale bar:50 μm **D** and **E** The data of staining intensity in immunohistochemical images are shown as mean ± SD. n = 5 for each group

Discussion

Exosomes, ranging from 30 to 150 nm, are small cargo-loaded EVs that originate from multivesicular bodies derived from endosomes. Naturally occurring exosomes derived from MSCs are the most extensively investigated therapeutic approach for OA due to their ease of acquisition and demonstrated efficacy. However, they also possess several limitations, including challenges in scaling up production and inadequate individual potency. Consequently, there has been a growing inclination towards engineering approaches in the realm of exosomes applications [10]. In this study, we found that TNF-α preconditioning enhanced exosome secretion in IPFP-MSCs through the activation of the PI3K/AKT pathway. Additionally, it induced the incorporation of chondroprotective LRP1 protein into exosomes, thereby exerted a beneficial effect on OA treatment in mice (Fig. 8). Therefore, this study presents a novel clinical treatment strategy for OA by investigating the functions and mechanisms of engineering exosomes from IPFP-MSCs in OA patients.

Previous studies have demonstrated that MSCs exhibit robust anti-inflammatory effects and possess exceptional immunomodulatory properties, primarily mediated through their paracrine actions [26, 27]. Recently, an increasing number of studies have demonstrated that exposure to a pro-inflammatory, such as LPS, or hypoxic preconditioned culture environment, can enhance the functional properties and paracrine effects of MSCs in combating chronic inflammatory conditions of OA [13, 28]. The proinflammatory cytokine TNF-α, which plays a pivotal role in the early stages of OA, is secreted and independently drives the inflammatory cascade [29]. Furthermore, TNF-α exerts an inhibitory effect on the adipogenic differentiation of human adipose-derived MSCs, thereby preserving their undifferentiated state [30, 31].

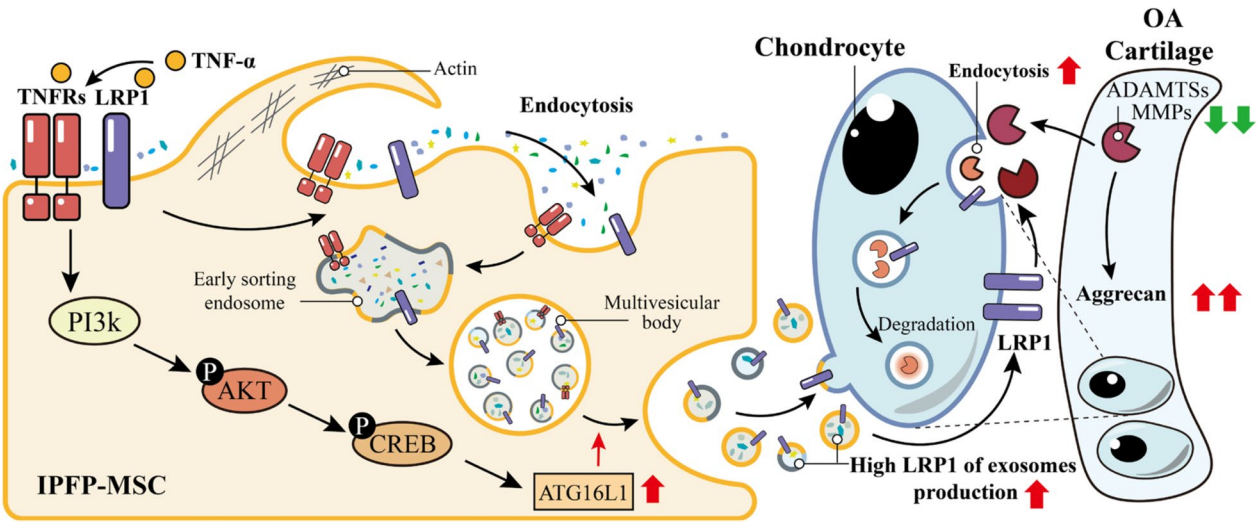

Fig. 8 Schematic Diagram: After TNF-α precondition, the PI3K/AKT signaling pathway within IPFP-MSCs is activated. This activation leads to the transcription factor CREB binding to the promoter region of ATG16L1, which promotes the transcription of ATG16L1, thereby increasing the release of exosomes. Concurrently, TNF-α treatment facilitates the enrichment of LRP1 in exosomes derived from IPFP-MSCs. When these LRP1-enriched exosomes are used to treat OA chondrocytes, they promote the degradation of ADAMTSs and MMPs within chondrocytes and increase Aggrecan levels in cartilage. Ultimately, this process favors the maintenance of the extracellular matrix homeostasis in OA cartilage

Based on the aforementioned findings, we employed TNF-α preconditioned IPFP-MSCs and observed a significant augmentation in exocrine secretion. A similar finding was reported, demonstrating that preconditioning MSCs with a pro-inflammatory cytokine cocktail consisting of IL-6, TNF-α, and IL-1β resulted in an approximately two-fold increase in exocrine secretion [32]. The findings presented here have significant implications for the future clinical application of exosomes derived from MSCs, especially in terms of scaling up production. Therefore, further investigation is needed to understand the underlying mechanism responsible for this observed effect.

Exosome biogenesis is a multistage process encompassing endocytosis, the establishment of the early endosome, progression to the late endosome, multivesicular body (MVB) formation, membrane fusion events, and ultimate exosome release [33]. Various proteins, such as members of the Rab protein family, autophagy-related proteins (ATGs), and SNARE proteins, play crucial roles in regulating the biogenesis and release of exosomes [34–36]. Upon activation, Rab5, a member of the Rab GTPase family, binds to the membranes of specific organelles due to its unique subcellular localization. This enables Rab5 to participate in a variety of membrane trafficking events, such as vesicle budding, intracellular vesicle transport, and membrane fusion processes. Rab27a is predominantly localized within CD63-positive MVBs and promotes their docking, tethering, and fusion with the plasma membrane through interaction with the effector protein Slp4 [34]. Rab7a is a key regulator that facilitates the maturation of endosomes and autophagosomes, guiding the transport of cargoes along microtubules and ultimately, participating in the fusion process with lysosomes (Maturation of autophagosomes and endosomes: A key role for Rab7) [37, 38]. SNAP23, a member of the SNARE complex, serves as a pivotal mediator in the fusion of MVBs and the subsequent release of exosomes [34, 39]. Additionally, autophagy is a lysosomal-dependent pathway for degradation and recycling. Recent studies have unveiled shared molecular machinery involved in exosome biogenesis and autophagy, as well as significant interplay between these two processes [40]. A previous study has demonstrated that exosome production is tightly regulated in cells through the ATG5-ATG16L1 complex, which de-acidifies multivesicular bodies via V_1V_0-ATPase [35]. In this study, we observed a significant up-regulation of mRNA expression levels in IPFP-MSCs following TNF-α preconditioning, including Rab5, ATG5 and ATG16L1. Based on RT-qPCR results showing a more pronounced fold change of ATG16L1 mRNA expression relative to Rab5 and ATG5, we elected to focus our subsequent experimental endeavors on ATG16L1. Nevertheless, it is noteworthy that Rab5 and ATG5 may also play a contributory role in TNF-α-induced exosome secretion from IPFP-MSCs, an aspect that necessitates comprehensive elucidation in future research. Furthermore, inhibition of ATG16L1 resulted in a significant decrease in the concentration of EVs derived from IPFP-MSCs. The PI3K/AKT kinase pathways play a pivotal

role in modulating the activation of autophagy in cells [41]. Previous studies have demonstrated that activation of the AKT/CREB signaling pathway, a crucial pro-survival signaling cascade, confers protection against stress-induced cellular apoptosis and inflammatory response [42, 43], while also playing a key role in the regulation of autophagy in neuronal cells [44]. The levels of p-AKT are significantly up-regulated in TNF-α preconditioned IPFP-MSCs, whereas inhibition of PI3K/AKT signaling leads to a reduction in the expression of ATG16L1. Furthermore, by integrating the findings from previous studies with our predictions, we postulate that the abundance of exocrine secretion in IPFP-MSCs following TNF-α preconditioning is partially attributed to the activation of AKT/CREB signaling pathway, leading to an up-regulation in ATG16L1 expression.

In our previous study, we found that exosomes derived from IPFP-MSCs alleviated gait abnormalities and exerted protective effects on the articular cartilage of OA [9]. We have presently discovered that the intra-articular administration of IPFP-MSC-EXOs$^{TNF-\alpha}$ exhibited superior efficacy in alleviating gait abnormalities and pathological changes compared to that of IPFP-MSC-EXOs^{naive} in the OA joint of mice. Further investigation into the underlying mechanism of enhanced therapeutic efficacy of exosomes derived from TNF-α preconditioned IPFP-MSCs revealed a significantly high expression of LRP1, a type I transmembrane protein that serves as the primary endocytic receptor for extracellular matrix-degrading MMPs and ADAMTSs in chondrocytes [15, 16], within these exosomes. One possible explanation is that the increase in LRP1 expression can be attributed to TNF-α preconditioning [45]. Moreover, LRP1 interacts with TNF receptor complexes to facilitate endocytosis and subsequent loading onto exosomes for secretion [46]. The intricate mechanism of these effect necessitates further investigation.

Recently, a study has reported that adipose-derived MSCs preconditioned with the pro-inflammatory factor IL-1β can produce chondroprotective EVs capable of crossing the complex cartilage matrix and rapidly penetrating to reach target chondrocytes [11]. We observed that the IPFP-MSC-EXOs$^{TNF-\alpha}$, which contains a high level of LRP1, effectively induces up-regulation of LRP1 expression in OA chondrocytes, thereby significantly alleviating the loss of cartilage ECMs. Relevant to our investigation, local inhibition of LRP1 shedding effectively restores the endocytic capacity and significantly mitigates aggrecan and collagen degradation in OA cartilage [47]. Notwithstanding the therapeutic advantages conferred by exosomal LRP1 derived from IPFP-MSC-EXOs$^{TNF-\alpha}$, delving into its potential as a clinical target for the amelioration of OA necessitates additional investigative efforts. Additionally, further research is necessary to thoroughly investigate other proteins or RNA components that are differentially present in IPFP-MSC-EXOs$^{TNF-\alpha}$.

While preconditioning MSCs with biochemical factors is a straightforward approach to augment exosome production without significant impact on their structures, it is imperative to acknowledge the potential cytotoxicity associated with the use of pro-inflammatory factors [10]. Additionally, distinct concentrations of TNF-α can exert divergent effects on the differentiation of MSCs [48]. In the future, further optimization of TNF-α preconditioning of MSCs is expected to yield enhanced and more robust outcomes. Despite TNF-α pretreatment upregulating LRP1 in exosomes derived from IPFP-MSCs, the loading efficiency remains inefficient. Therefore, the methods for engineering exosomes to enhance their protein loading efficiency are worth considering. For example, engineered EVs that deliver therapeutic protein cargoes using self-assembling "enveloped protein nanocages" (EPN) may provide an effective solution in the future [49]. In summary, preconditioning with TNF-α activates the PI3K/AKT signaling pathway in IPFP-MSCs, leading to the upregulation of ATG16L1 levels. Consequently, this enhances the production of LRP1-enriched exosomes, which serve as protective agents against cartilage damage caused by OA. This approach presents a compelling alternative for engineering MSC-derived exosomes as a therapeutic strategy for OA.

Abbreviations

ADAMTSs	A disintegrin and metalloproteinase with thrombospondin motifs
ATG16L1-RNAi	autophagy-related protein 16 like 1-silencing RNA
CREB	Cyclic AMP-responsive element binding protein
DMEM	Dulbecco's modified Eagle's medium
DMM	Destabilization of the medial meniscus
ECM	Extracellular matrix
EVs	Extracellular vesicles
FBS	Fetal bovine serum
GO	Gene Ontology
IPFP	Infrapatellar fat pad
IPFP-MSC-EXOs	Exosomes derived from IPFP-MSCs
IPFP-MSC-EXOs^{naive}	Exosomes derived from naive IPFP-MSCs
IPFP-MSC-EXOs$^{TNF-\alpha}$	Exosomes derived from TNF-α preconditioned IPFP-MSCs
KEGG	Kyoto Encyclopedia of Genes and Genomes
LC–MS/MS	Liquid chromatography tandem mass spectrometry
LRP1	Lipoprotein receptor-related protein 1
LPS	Lipopolysaccharide
MSCs	Mesenchymal stem cells
MMPs	Matrix metalloproteinases
NTA	Nanoparticle tracking analysis
OA	Osteoarthritis
OARSI	Osteoarthritis Research Society International
PBS	Phosphate-buffered saline
TEM	Transmission electron microscopy
TKA	Total knee replacement

Acknowledgements
The authors thank Prof. Baorong Liu of Hunan Provincial People's Hospital for his guidance and support in this study. We also thank Prof. Zhan Li and Prof. Liang Kuang of Army Medical University for their guidance and help in the experiment. I would like to express our gratitude to the department of clinical biochemistry, department of stem cell and regenerative medicine, and center of bone metabolism and repair of army medical university for their support with experimental equipment and platforms.

Author contributions
ZH N, JY W, YQ W, and JH W participated in the conceptualization and designing of this study. JH W, JY W, W X, YQ G, DB F, SZ F and YR W performed the experiments, and JY W, SR Z, JH W, ZH N and Z L wrote the manuscript. SR Z, JH W, ZH N, W X, Y L, R C, X Z, BF Z and LF C provided suggestions and performed the analysis. SR Z, S L, B Z, TY Z and L Y offered suggestions for revisions and polished the article. JY W , ZH N, W X, JH W, YZ Z, YQ W, S H, R C, NN L, H X and JQ L participated in the interpretation of the results. All authors read and approved the final submitted manuscript.

Funding
National Natural Science Foundation of China (No. 82002305, No. 82372495, No. 81871817, No. 82202770, No.81802205); Natural Science Foundation of Chongqing Municipality (No. CSTB2022NSCQ-MSX1267, No. CSTB2022NSCQ-MSX0863); Innovative Capability Enhancement program of Army Medical Center of PLA (No. ZXYZZKY01); Chongqing Acute and Critical Care Clinical Medical Research Center (No. 3354181); Beijing Municipal Science Technology Commission (No. Z221100007422039); and Chongqing Municipal Healthcare Technology Promotion Project (No. 2020jstg028).

Availability of data and materials
No datasets were generated or analysed during the current study.

Declarations

Ethics approval and consent to participate
This study was approved by the Ethics Committee of Army Medical University Daping Hospital.

Consent for publication
Not applicable.

Competing interests
The authors declare no competing interests.

Author details
[1]Plastic Surgery Hospital, Chinese Academy of Medical Sciences and Peking Union Medical College, Beijing 100144, China. [2]Department of Joint Surgery and Sport Medicine, Hunan Provincial People's Hospital, The First Affiliated Hospital of Hunan Normal University, Changsha 410000, China. [3]Department of Rehabilitation Medicine, Daping Hospital, Army Medical University, Chongqing 400022, China. [4]Department of Orthopedics, Shanghai Hospital, Wanzhou District, Chongqing 40400, China. [5]Department of Clinical Biochemistry, Faculty of Pharmacy and Laboratory Medicine, Army Medical University, Gantaoyan Street, Shapinba District, Chongqing 400038, China. [6]War Trauma Medical Center, State Key Laboratory of Trauma and Chemical Poisoning, Army Medical Center, Daping Hospital, Army Medical University, Chongqing 40038, People's Republic of China. [7]Center of Bone Metabolism and Repair, Laboratory for Prevention and Rehabilitation of Training Injuries, State Key Laboratory of Trauma, Burns and Combined Injury, Trauma Center, Research Institute of Surgery, Daping Hospital, Army Medical University (Third Military Medical University), Chongqing 400000, China. [8]Rehabilitation Center, Strategic Support Force Xingcheng Special Duty Sanatorium, Xingcheng 125105, China. [9]Department of General Practice, Chinese PLA General Hospital of the Central Theater Command, Wuhan 430012, China. [10]Department of Laboratory Medicine, The Fifth Clinical Medical College of, Henan University of Chinese Medicine (Zhengzhou People's Hospital), Zhengzhou 450003, China. [11]Department of Laboratory Medicine, The Third Affiliated Hospital of Zhengzhou University, Zhengzhou 450003, China.

Received: 20 March 2024 Accepted: 20 August 2024
Published online: 11 September 2024

References

1. Tong L, et al. Current understanding of osteoarthritis pathogenesis and relevant new approaches. Bone Res. 2022;10(1):60.
2. Hunter DJ, Bierma-Zeinstra S. Osteoarthritis. Lancet. 2019;393(10182):1745–59.
3. Bornes TD, Adesida AB, Jomha NM. Mesenchymal stem cells in the treatment of traumatic articular cartilage defects: a comprehensive review. Arthritis Res Ther. 2014;16(5):432.
4. Johnson K, et al. A stem cell-based approach to cartilage repair. Science. 2012;336(6082):717–21.
5. Moradi L, et al. Regeneration of meniscus tissue using adipose mesenchymal stem cells-chondrocytes co-culture on a hybrid scaffold: In vivo study. Biomaterials. 2017;126:18–30.
6. Malhotra K, et al. Combinatorial effect of biomaterials and extracellular vesicle therapy for heart failure with reduced ejection fraction: a systematic review of preclinical studies. Adv Healthc Mater. 2023;12(32): e2301980.
7. Xiong Y, Mahmood A, Chopp M. Mesenchymal stem cell-derived extracellular vesicles as a cell-free therapy for traumatic brain injury via neuroprotection and neurorestoration. Neural Regen Res. 2024;19(1):49–54.
8. Bertolino GM, et al. Therapeutic potential in rheumatic diseases of extracellular vesicles derived from mesenchymal stromal cells. Nat Rev Rheumatol. 2023;19(11):682–94.
9. Wu J, et al. miR-100-5p-abundant exosomes derived from infrapatellar fat pad MSCs protect articular cartilage and ameliorate gait abnormalities via inhibition of mTOR in osteoarthritis. Biomaterials. 2019;206:87–100.
10. Liu Z, et al. Breakthrough of extracellular vesicles in pathogenesis, diagnosis and treatment of osteoarthritis. Bioact Mater. 2023;22:423–52.
11. Colombini A, et al. Adipose-derived mesenchymal stromal cells treated with interleukin 1 beta produced chondro-protective vesicles able to fast penetrate in cartilage. Cells. 2021;10:5.
12. Kim M, et al. Exosomes from IL-1β-primed mesenchymal stem cells inhibited IL-1β- and TNF-α-mediated inflammatory responses in osteoarthritic SW982 Cells. Tissue Eng Regen Med. 2021;18(4):525–36.
13. Duan A, et al. Extracellular vesicles derived from LPS-preconditioned human synovial mesenchymal stem cells inhibit extracellular matrix degradation and prevent osteoarthritis of the knee in a mouse model. Stem Cell Res Ther. 2021;12(1):427.
14. Molnar V, et al. Cytokines and chemokines involved in osteoarthritis pathogenesis. Int J Mol Sci. 2021;22:17.
15. Yamamoto K, et al. MMP-13 is constitutively produced in human chondrocytes and co-endocytosed with ADAMTS-5 and TIMP-3 by the endocytic receptor LRP1. Matrix Biol. 2016;56:57–73.
16. Yamamoto K, et al. LRP-1-mediated endocytosis regulates extracellular activity of ADAMTS-5 in articular cartilage. Faseb j. 2013;27(2):511–21.
17. Kuang L, et al. FGFR3 deficiency enhances CXCL12-dependent chemotaxis of macrophages via upregulating CXCR7 and aggravates joint destruction in mice. Ann Rheum Dis. 2020;79(1):112–22.
18. Bencze J, et al. Comparison of semi-quantitative scoring and artificial intelligence aided digital image analysis of chromogenic immunohistochemistry. Biomolecules. 2021;12:1.
19. Du K, Montminy M. CREB is a regulatory target for the protein kinase Akt/PKB. J Biol Chem. 1998;273(49):32377–9.
20. Zarneshan SN, Fakhri S, Khan H. Targeting Akt/CREB/BDNF signaling pathway by ginsenosides in neurodegenerative diseases: a mechanistic approach. Pharmacol Res. 2022;177: 106099.
21. Wan X, et al. AKT1-CREB stimulation of PDGFRα expression is pivotal for PTEN deficient tumor development. Cell Death Dis. 2021;12(2):172.
22. Chen L, et al. Long term usage of dexamethasone accelerating accelerates the initiation of osteoarthritis via enhancing chondrocyte apoptosis and the extracellular matrix calcification and apoptosis of chondrocytes. Int J Biol Sci. 2021;17(15):4140–53.
23. Gharbi SI, et al. Exploring the specificity of the PI3K family inhibitor LY294002. Biochem J. 2007;404(1):15–21.

24. Glasson SS, et al. The OARSI histopathology initiative - recommendations for histological assessments of osteoarthritis in the mouse. Osteoarthritis Cartilage. 2010;18(Suppl 3):S17-23.
25. Krenn V, et al. Synovitis score: discrimination between chronic low-grade and high-grade synovitis. Histopathology. 2006;49(4):358–64.
26. Takizawa N, et al. Bone marrow-derived mesenchymal stem cells propagate immunosuppressive/anti-inflammatory macrophages in cell-to-cell contact-independent and -dependent manners under hypoxic culture. Exp Cell Res. 2017;358(2):411–20.
27. Zhang S, et al. MSC exosomes mediate cartilage repair by enhancing proliferation, attenuating apoptosis and modulating immune reactivity. Biomaterials. 2018;156:16–27.
28. Rong Y, et al. Hypoxic pretreatment of small extracellular vesicles mediates cartilage repair in osteoarthritis by delivering miR-216a-5p. Acta Biomater. 2021;122:325–42.
29. Ding X, et al. Cadherin-11 involves in synovitis and increases the migratory and invasive capacity of fibroblast-like synoviocytes of osteoarthritis. Int Immunopharmacol. 2015;26(1):153–61.
30. Lencel P, et al. TNF-α stimulates alkaline phosphatase and mineralization through PPARγ inhibition in human osteoblasts. Bone. 2011;48(2):242–9.
31. Ma H, et al. Macrophages inhibit adipogenic differentiation of adipose tissue derived mesenchymal stem/stromal cells by producing pro-inflammatory cytokines. Cell Biosci. 2020;10:88.
32. Tolomeo AM, et al. Extracellular vesicles secreted by mesenchymal stromal cells exert opposite effects to their cells of origin in murine sodium dextran sulfate-induced colitis. Front Immunol. 2021;12: 627605.
33. Ni Z, et al. Exosomes: roles and therapeutic potential in osteoarthritis. Bone Res. 2020;8:25.
34. Xu M, et al. The biogenesis and secretion of exosomes and multivesicular bodies (MVBs): Intercellular shuttles and implications in human diseases. Genes Dis. 2023;10(5):1894–907.
35. Guo H, et al. Atg5 disassociates the V(1)V(0)-ATPase to promote exosome production and tumor metastasis independent of canonical macroautophagy. Dev Cell. 2017;43(6):716-730.e7.
36. Murrow L, Malhotra R, Debnath J. ATG12-ATG3 interacts with Alix to promote basal autophagic flux and late endosome function. Nat Cell Biol. 2015;17(3):300–10.
37. Guerra F, et al. Modulation of RAB7A protein expression determines resistance to cisplatin through late endocytic pathway impairment and extracellular vesicular secretion. Cancers. 2019;11:1.
38. Tan EHN, B.L. Tang, Rab7a and mitophagosome formation. Cells. 2019;8:3.
39. Verweij FJ, et al. Quantifying exosome secretion from single cells reveals a modulatory role for GPCR signaling. J Cell Biol. 2018;217(3):1129–42.
40. Xu J, Camfield R, Gorski SM. The interplay between exosomes and autophagy - partners in crime. J Cell Sci. 2018;131:15.
41. Ceccariglia S, et al. Autophagy: a potential key contributor to the therapeutic action of mesenchymal stem cells. Autophagy. 2020;16(1):28–37.
42. Hu M, et al. Autophagy and Akt/CREB signalling play an important role in the neuroprotective effect of nimodipine in a rat model of vascular dementia. Behav Brain Res. 2017;325(Pt A):79–86.
43. Herkel J, et al. Activation of the Akt-CREB signalling axis by a proline-rich heptapeptide confers resistance to stress-induced cell death and inflammation. Immunology. 2017;151(4):474–80.
44. Carloni S, et al. Activation of autophagy and Akt/CREB signaling play an equivalent role in the neuroprotective effect of rapamycin in neonatal hypoxia-ischemia. Autophagy. 2010;6(3):366–77.
45. Campana WM, et al. The low-density lipoprotein receptor-related protein is a pro-survival receptor in Schwann cells: possible implications in peripheral nerve injury. J Neurosci. 2006;26(43):11197–207.
46. Gaultier A, et al. Regulation of tumor necrosis factor receptor-1 and the IKK-NF-kappaB pathway by LDL receptor-related protein explains the antiinflammatory activity of this receptor. Blood. 2008;111(11):5316–25.
47. Yamamoto K, et al. Inhibition of shedding of low-density lipoprotein receptor-related protein 1 reverses cartilage matrix degradation in osteoarthritis. Arthritis Rheumatol. 2017;69(6):1246–56.
48. Li W, et al. The role of TNF-α in the fate regulation and functional reprogramming of mesenchymal stem cells in an inflammatory microenvironment. Front Immunol. 2023;14:1074863.
49. Ovchinnikova LA, et al. Reprogramming extracellular vesicles for protein therapeutics delivery. Pharmaceutics. 2021;13:6.

Publisher's Note